Available online at www.sciencedirect.com

SciVerse ScienceDirect

Ceramics International 38 (2012) 6579–6584

CERAMICS INTERNATIONAL

www.elsevier.com/locate/ceramint

Water-soluble, mesoporous Fe_3O_4: Synthesis, characterization, and properties

S. Asuha*, H.L. Wan, S. Zhao, W. Deligeer, H.Y. Wu, L. Song, O. Tegus

Chemistry & Environment Science College, Inner Mongolia Normal University, and Key Laboratory of Physics and Chemistry of Functional Materials, Inner Mongolia, 81 Zhaowudalu, Huhhot 010022, China

Received 3 February 2012; received in revised form 21 April 2012; accepted 14 May 2012
Available online 22 May 2012

Abstract

Water-soluble, mesoporous Fe_3O_4 nanopowder is successfully prepared by one-step thermal decomposition of an iron-urea complex ($[Fe(NH_2CONH_2)_6](NO_3)_3$) in triethylene glycol (TEG). The formation of Fe_3O_4 is confirmed from X-ray diffraction (XRD), X-ray photoelectron spectroscopy (XPS), and selected area electron diffraction (SAED) measurements. The morphological and structural properties of the Fe_3O_4 nanopowder are characterized by transmission electron microscopy (TEM), nitrogen adsorption–desorption, and thermogravimetric analysis (TGA). Monodisperse, nearly spherical and highly crystalline Fe_3O_4 nanoparticles are obtained by this method. The Fe_3O_4 nanopowder is well dispersed in water and ethanol with a mesoporous structure, average pore size of 3.6 nm, and Brunauner–Emmett–Teller (BET) surface area of 122 m^2/g. The room temperature magnetization hysteresis curve exhibits barely measurable values for coercivity and remanence, suggesting that the Fe_3O_4 nanopowder possesses superparamagnetic characteristics.

Keywords: Magnetite; Water-soluble; Mesoporous; Thermal decomposition

1. Introduction

Magnetite (Fe_3O_4) nanopowder has shown great potential in many applications such as ferro-fluids, catalysis, magnetic separation, drug delivery, and magnetic resonance imaging [1–6]. For all these applications, high quality Fe_3O_4 nanopowder with different properties is required to satisfy individual demands. For example, in biomedical applications, Fe_3O_4 nanopowder is required to be monodisperse and soluble in water in order to provide good biocompatibility. For applications in ferro-fluids and catalysis, it is also required to have good dispersivity in commonly used solvents (e.g., water, ethanol, hexane, etc.). With regard to the many potential applications of Fe_3O_4 nanopowder, various preparation methods have been developed, such as co-precipitation, microemulsion, hydrothermal method, sonochemical approach, electrospray synthesis, and high-temperature organic phase decomposition [7–12]. Among these methods, the high-temperature organic phase decomposition method has recently been proven to be a promising synthetic route for preparing monodisperse Fe_3O_4 nanopowder. In 1999, Rockenberger et al. [13] first demonstrated that a transition metal oxide nanopowder with a narrow size distribution could be synthesized by thermal decomposition of metal cupferron complexes in long-chain amines. Subsequently, there have been many successful attempts to apply this methodology for the synthesis of monodisperse iron oxide nanopowder. Hyeon et al. [14] have successfully prepared monodisperse γ-Fe_2O_3 nanopowder by the oxidative thermal decomposition of iron pentacarbonyl ($Fe(CO)_5$) in octyl ether in the presence of oleic acid. Sun and Zeng [15] reported the formation of monodisperse Fe_3O_4 nanopowder by the high-temperature reaction of iron (III) acetylacetonate in the presence of alcohol, oleic acid, and oleylamine. Jana et al. [16] synthesized nearly monodisperse Fe_3O_4 nanopowder having particles in a large range of sizes (3–50 nm) by the pyrolysis of iron oleate complexes in octadecene.

*Corresponding author. Tel.: +86 471 43921214; fax: +86 471 4392124.
E-mail addresses: asuha42@yahoo.com.cn, asuha@imnu.edu.cn (S. Asuha).

0272-8842/$36.00
http://dx.doi.org/10.1016/j.ceramint.2012.05.042

However, all these methods have multiple steps, use multiple reagents, and yield Fe_3O_4 nanopowder that is only soluble in some nonpolar solvents.

The polyol method is a versatile chemical approach that has recently been applied to synthesize monodisperse nanoscale oxide particles [17]. In this method, oxide nanopowder is formed by the thermal decomposition of corresponding metal salts in polyol (i.e., polyalcohol) solvents. Since polyol is hydrophilic, highly water-soluble nanopowder can be synthesized by using the polyol method. Wan et al. prepared water-soluble ~8 nm Fe_3O_4 nanopowder by using this method [18,19]. Hu et al. reported the synthesis of monodisperse, water-soluble, 3–6 nm Fe_3O_4 nanopowder with diethylene glycol (DEG) as the solvent [20].

As previously reported, toxic organic iron complexes (e.g., $Fe(CO)_5$, iron acetylacetonate, and iron cupferronates) are commonly used as precursors in the high-temperature organic phase decomposition method. These compounds are undesirable for the mass production of Fe_3O_4 nanopowder because of their toxicity and instability. Therefore, an inexpensive, safe, and stable chemical is needed for use as a starting material in the synthesis of Fe_3O_4 nanopowder. A further challenge is the preparation of water-soluble Fe_3O_4 nanopowder with large surface area via a simple synthetic route. In this work, we show that water-soluble, mesoporous Fe_3O_4 nanopowder with a relatively high surface area can be prepared via one-step thermal decomposition of $[Fe(NH_2CONH_2)_6](NO_3)_3$ in triethylene glycol (TEG). In comparison with organic iron complexes that are currently used as precursors in thermal decomposition process, $[Fe(NH_2CONH_2)_6](NO_3)_3$ is a nontoxic, stable inorganic complex, as shown from its application in agriculture as a fertilizer [21]; hence, it can be safely used as an iron oxide precursor. Interestingly, the Fe_3O_4 nanopowder prepared by this method possesses a mesoporous structure with a large surface area. Owing to these excellent surface properties, the mesoporous Fe_3O_4 is a promising material for the separation of target molecules from a multiphase complex system and the removal of pollutants from waste water with an external magnetic device [22].

2. Experimental

2.1. Materials

$Fe(NO_3)_3 \cdot 9H_2O$ (99%, Tianjin Fengchuan Chemical Reagents Company), urea (99%, Tianjin ShengAo Chemical Reagents Company), absolute ethanol (99%, Beijing Chemical Reagents Company), and triethylene glycol (99%, Tianjin Guangfu Chemical Reagents Company) were used as received.

2.2. Synthesis

The synthesis of Fe_3O_4 nanopowder is as follows. 8.0 g of $[Fe(NH_2CONH_2)_6](NO_3)_3$ synthesized using a previously reported method [23] was mixed with 50 mL of TEG in a beaker under magnetic stirring. The solution was transferred into a three-neck flask equipped with a condenser. It was then slowly heated to 260 °C and kept at that temperature for 5 h, resulting in the formation of a black homogeneous colloidal suspension. After cooling to room temperature, 20 mL of ethyl acetate was added to the suspension under vigorous stirring, and then, the black precipitate was magnetically separated from the solution. This ethyl acetate washing and magnetic separation procedure was repeated five times to remove TEG from the Fe_3O_4 nanopowder product. Finally, the precipitate was dried in a vacuum desiccator to yield a solid product.

2.3. Characterization

X-ray diffraction (XRD) patterns were recorded on a Rigaku D/Max 2500 V/PC diffractometer with CuKα radiation. X-ray photoelectron spectroscopy (XPS) spectra were measured using a VG ESCALAB-MKII 250 instrument with a monochromatic Al Kα radiation source. The obtained peaks were calibrated using the C 1s peak. Transmission electron micrograph (TEM) and selected area electron diffraction (SAED) measurements were carried out using a JEOL JEM-2200FS high-resolution transmission electron microscope. Nitrogen adsorption–desorption isotherms were measured using a Micrometrics ASAP2020 Analyzer. Thermogravimetric analysis (TGA) and differential thermal analysis (DTA) were carried out at a heating rate of 5 °C/min from room temperature to 500 °C using a Shimadzu DTG-60H apparatus. The FTIR spectra were recorded using a Nicolet Nexus 670 spectrometer in dry-nitrogen atmosphere. Magnetic measurements were performed using a Lake Shore 7407 vibrating-sample magnetometer (VSM) at room temperature.

3. Results and discussion

Fig. 1 shows the XRD pattern of the powder prepared by thermal decomposition of $[Fe(NH_2CONH_2)_6](NO_3)_3$ in TEG at 260 °C for 5 h. The diffraction pattern matches well with the JCPDS file (e.g., No. 19-0629) of Fe_3O_4, thus indicating the formation of Fe_3O_4. The γ-Fe_2O_3 is one of the iron oxides with a cubic spinel crystalline structure, and its XRD patterns are similar to those of Fe_3O_4. Therefore, it is very difficult to differentiate between these materials solely from their diffraction patterns. Recently, XPS has been proven to be a powerful and convenient tool for the discrimination of Fe_3O_4 and γ-Fe_2O_3, mainly because this technique is very sensitive to Fe^{3+} and Fe^{2+} [24,25]. In this study, XPS analysis confirmed the formation of Fe_3O_4. Fig. 2 shows the XPS spectrum in the Fe 2p region for the sample. The peak positions of Fe $2p_{3/2}$ and Fe $2p_{1/2}$ were observed at 710.5 and 723.8 eV, respectively; these values agree well with those for Fe_3O_4 reported in literature [26]. Besides peak position, the satellite peak of Fe $2p_{3/2}$ is also very sensitive to the oxidation states of Fe. The Fe $2p_{3/2}$ for Fe_3O_4 does not have any satellite peaks, while that for

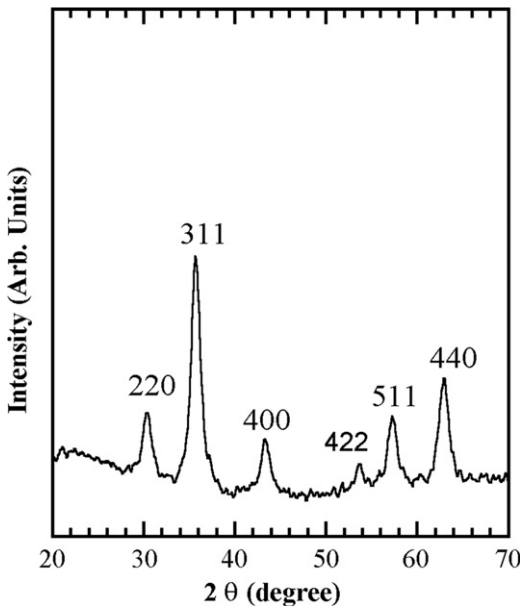

Fig. 1. XRD pattern of the sample prepared by the thermal decomposition of $[Fe(NH_2CONH_2)_6](NO_3)_3$ in TEG at 260 °C for 5 h.

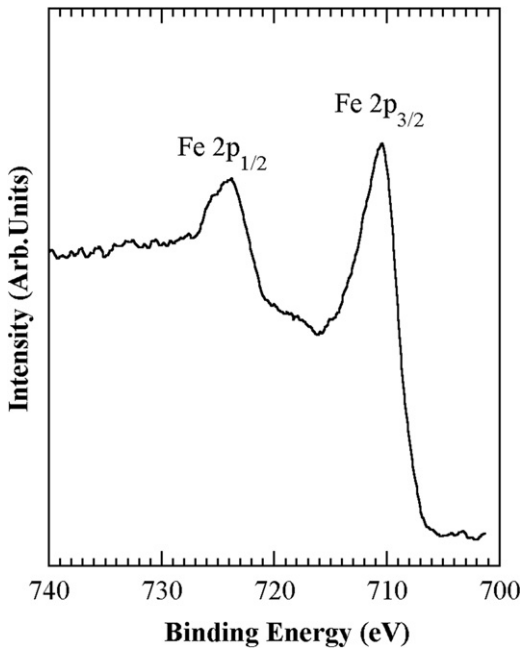

Fig. 2. XPS spectrum of the sample prepared by the thermal decomposition of $[Fe(NH_2CONH_2)_6](NO_3)_3$ in TEG at 260 °C for 5 h.

γ-Fe_2O_3 has a satellite peak at ~719 eV. The absence of the satellite peak in the XPS spectrum reveals that our sample is Fe_3O_4. The TEM micrograph of the Fe_3O_4 nanopowder is shown in Fig. 3a. As seen in the figure, the Fe_3O_4 particles were nearly spherical and monodisperse with an average size of around 7 nm. Fig. 3b shows the HRTEM image of a single particle. These particles were single crystalline, as shown clearly by atomic lattice fringes. The distance between the two adjacent planes was 0.49 nm, which corresponds to a lattice spacing of (111) planes of Fe_3O_4 with a spinel structure. The SAED patterns of the sample are shown in Fig. 3c. The presence of rings in the electron diffraction patterns is indicative of the crystalline nature of the particles and can be indexed to Fe_3O_4.

The mechanism of Fe_3O_4 formation can be understood from the thermal decomposition reaction of $[Fe(NH_2CONH_2)_6](NO_3)_3$. According to our previous study, the thermal decomposition reaction involves a two-stage decomposition process, and $Fe(NO_3)_3$ and urea (NH_2CONH_2) are the main products in the first step as expressed by the following equation [27]:

$$[Fe(NH_2CONH_2)6](NO_3)_3 \rightarrow Fe(NO_3)_3 + 6NH_2CONH_2 \quad \text{(first stage)} \quad (1)$$

This stage occurs in the temperature range of 180–196 °C. Further evidence of the release of NH_2CONH_2 in this step was also obtained from infrared spectroscopy. Fig. 4 shows the FTIR spectra of NH_2CONH_2 (spectrum a) and the gaseous product that was collected on a condenser during the thermal decomposition process (spectrum b). The absorption peaks at 3447, 3346, 1675, 1466, and 1154 cm^{-1} are the characteristic absorption peaks of NH_2CONH_2. They are attributable to the asymmetric stretching vibration of N–H, symmetric stretching vibration of N–H, bending vibration of N–H, stretching vibration of C–N, and rocking vibration of N–H, respectively. The similarity of the two spectra demonstrates that the gaseous product is NH_2CONH_2. Fig. 5 shows the DTA curves of $[Fe(NH_2CONH_2)_6](NO_3)_3$ and NH_2CONH_2. The endothermic peaks at ~186 °C (curve a) and ~140 °C (curve b) are due to the melting of $[Fe(NH_2CONH_2)_6](NO_3)_3$ and NH_2CONH_2, respectively. The strong exothermic peak at 197.4 °C (curve a) and the endothermic peak at 215.5 °C (curve b) are attributable to the first stage decompositions of $[Fe(NH_2CONH_2)_6](NO_3)_3$ and NH_2CONH_2, respectively, indicating that the thermal decomposition temperature of $[Fe(NH_2CONH_2)_6](NO_3)_3$ is lower than that of NH_2CONH_2. The result suggests that the NH_2CONH_2 produced from the first stage decomposition of $[Fe(NH_2CONH_2)_6](NO_3)_3$ could react with Fe^{3+} in the next step.

NH_2CONH_2 is a reducing agent, and it can partially reduce Fe^{3+} to Fe^{2+}, leading to the formation of Fe_3O_4. This suggests that the products of the second stage are likely to depend on heat treatment atmosphere. When the thermal decomposition of $[Fe(NH_2CONH_2)_6](NO_3)_3$ is carried out in an open container (i.e., in air), the NH_2CONH_2 released in the first stage will be separated from $Fe(NO_3)_3$ by evaporation. Therefore, no reduction of Fe^{3+} occurs. In that case, the thermal decomposition of $[Fe(NH_2CONH_2)_6](NO_3)_3$ will yield γ-Fe_2O_3, as shown in our previous studies [23]. In the current case where the thermal decomposition reaction proceeds in TEG, however, the NH_2CONH_2 released in the first stage could not escape from the reactor under reflux, thus leading to the formation of Fe_3O_4.

$$Fe(NO_3)_3 + NH_2CONH_2 \rightarrow Fe_3O_4 + CO_2 + 4NO + 7NO_2 + O_2 + 2H_2 \quad \text{(second stage)} \quad (2)$$

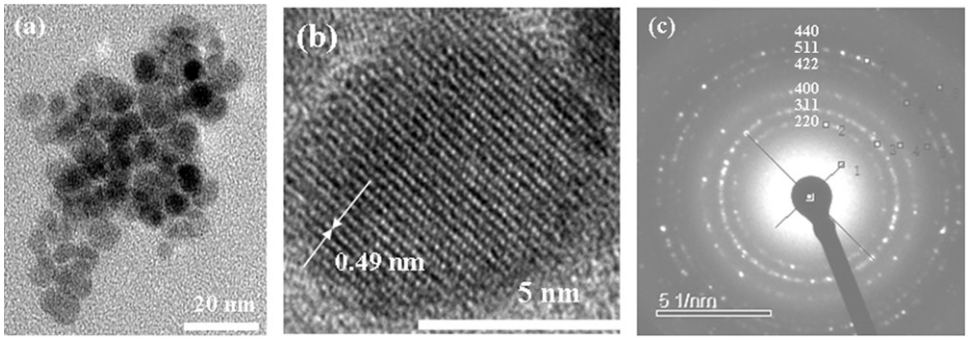

Fig. 3. (a) TEM image, (b) HRTEM image and (c) SAED patterns of the Fe_3O_4 nanopowder.

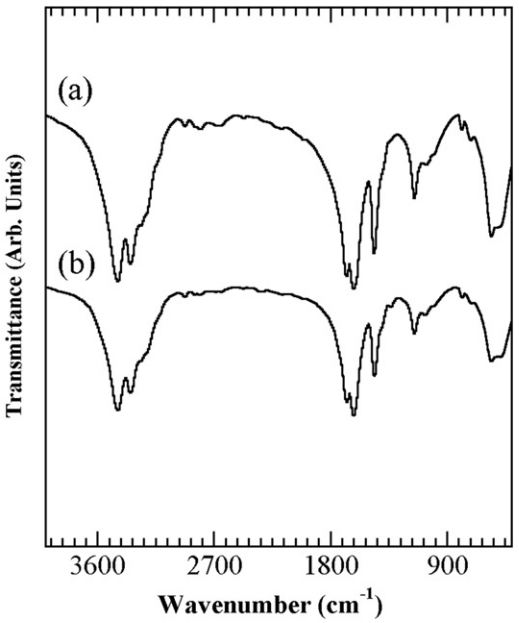

Fig. 4. FTIR spectra (a) for the urea and (b) for the thermal decomposition product of $[Fe(NH_2CONH_2)_6](NO_3)_3$.

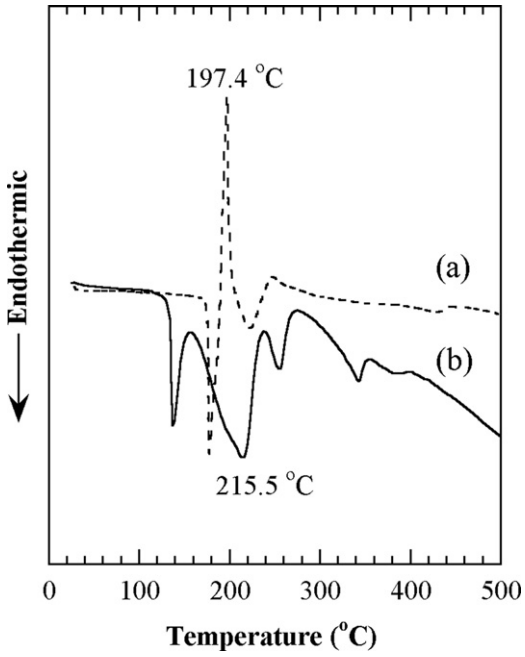

Fig. 5. DTA curves for $[Fe(NH_2CONH_2)_6](NO_3)_3$ (a) and urea (b).

According to Eq. (2), one NH_2CONH_2 molecule is required for three $Fe(NO_3)_3$ to produce Fe_3O_4. In this case, excess NH_2CONH_2 will thermally decompose with a further increase in solution temperature and will be removed from solution. On the other hand, it has been demonstrated that polyol can act as a reducing agent. Thus, TEG may also partially reduce Fe^{3+} to Fe^{2+}, forming Fe_3O_4 [17]. The reason for the formation of monodisperse small Fe_3O_4 particles could be explained from the correlation between crystal nucleation and crystal growth processes. It is known that the size and the morphology of the particles depend strongly on the competition between crystal nucleation and crystal growth. When the rate of crystal nucleation is greater than that of crystal growth, small particles with a low aspect ratio will be obtained. In this example, the thermal decomposition of $[Fe(NH_2CONH_2)_6](NO_3)_3$ is a fast step, and it may induce rapid crystal nucleation. Hence, we believe that the formation of monodisperse small Fe_3O_4 particles is attributable to the rapid crystal nucleation. In addition, in this method, TEG acts as a stabilizer to suppress the growth of particles and prevent their agglomeration.

Fig. 6 shows the nitrogen adsorption–desorption isotherm of the Fe_3O_4 nanopowder. The inset shows the Barrett–Joyner–Halenda (BJH) pore size distribution plot. The shape and hysteresis loop are similar to a standard type IV isotherm [28], indicating that the aggregates of Fe_3O_4 particles possess a mesoporous structure. At the same time, the BJH curve reveals that the mesoporous Fe_3O_4 nanopowder has a narrow distribution of pore sizes centered at 3.6 nm. From the adsorption isotherm, the BET surface area of the sample was estimated to be 122 m^2/g. This value is much larger than those obtained for previously reported mesoporous Fe_3O_4 [22,29]. In general, a soft or hard template is necessary for the formation of a mesoporous structure because a pore is formed via the extraction of the template. In this case, however, no template was used in the synthesis of the Fe_3O_4 nanopowder. It is highly probable that the pores in the mesoporous range are formed via the agglomeration of

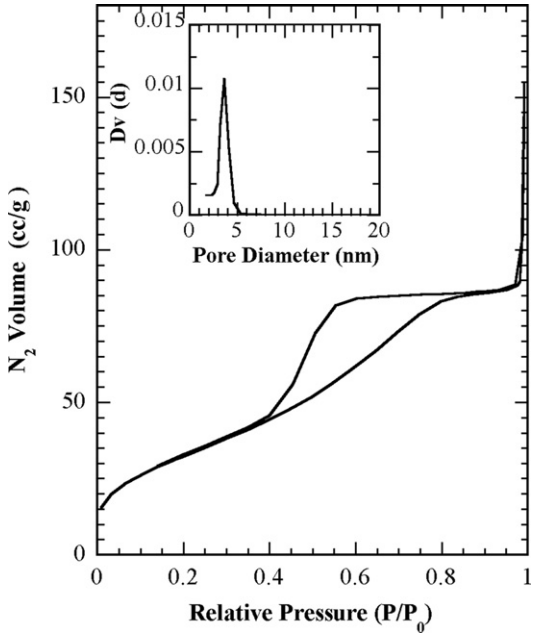

Fig. 6. Nitrogen adsorption–desorption isotherm of Fe_3O_4 nanopowder. The BJH curve of the sample is shown in the inset.

primary Fe_3O_4 particles, and thus, the uniform sizes of the primary particles may lead to the formation of mesopores with a narrow pore size distribution. On the other hand, several kinds of gaseous species including CO_2, NO, NO_2, and O_2 are formed as by-products in the thermal decomposition process of $[Fe(NH_2CONH_2)_6](NO_3)_3$ according to Eq. (2). Hence, the mesopores in the sample may also be formed via the removal of these gaseous species.

The obtained Fe_3O_4 nanopowder was readily dispersed in water and ethanol, and, the resulting colloidal suspensions can be kept for more than several months without noticeable precipitation. The TGA curve of the Fe_3O_4 nanopowder is shown in Fig. 7. A two-stage weight loss where the first stage occurred in the temperature range 20–200 °C and the second in the range 200–360 °C was observed in the TGA curve. The total weight loss was ~12%. The weight losses in the first stage and the second stage were attributed to the removal of ethyl acetate (or water) and TEG molecules, respectively, demonstrating the presence of TEG molecules on the Fe_3O_4 particle surface. Therefore, the high water solubility of the Fe_3O_4 nanopowder may arise from the hydrophilic property of TEG molecules adhering to the particle surface.

Fig. 8 shows the room temperature magnetization hysteresis curve of the Fe_3O_4 nanopowder. The inset is an enlarged hysteresis curve that shows almost immeasurable values of coercivity and remanence, suggesting that the Fe_3O_4 nanopowder possesses superparamagnetic characteristics at room temperature. This result agrees with the fact that the critical Fe_3O_4 particle size below which a superparamagnetic behavior will be observed is ~29 nm [30]. The magnetization (M) of the sample did not show a saturation value. The maximum M obtained at 15 kOe was 36.8 emu/g, which was much smaller than that of bulk

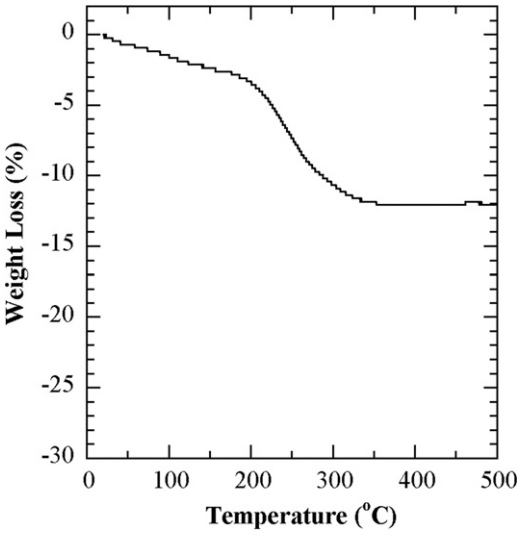

Fig. 7. TGA curve of the Fe_3O_4 nanopowder.

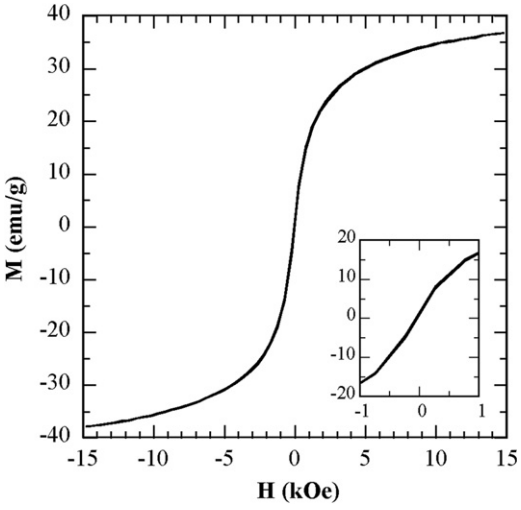

Fig. 8. Room temperature magnetization hysteresis curve of the Fe_3O_4 nanopowder. An enlarged hysteresis curve is shown in the inset.

Fe_3O_4 crystallite (i.e., ~92 emu/g). This phenomenon has also been reported previously [31,32]. As mentioned earlier, the Fe_3O_4 nanopowder was coated with a TEG layer, and this non-magnetic layer is thought to be one of the most probable reasons for the reduction in the maximum M. Considering the weight loss of ~12%, the normalized maximum M is estimated to be 42 emu/g. This value is still much smaller than that of bulk Fe_3O_4 crystallite, probably because of a surface spin canting effect [33].

4. Conclusions

A polyol method has been used to synthesize Fe_3O_4 nanopowder. This synthetic route yields water-soluble, monodisperse, mesoporous, and superparamagnetic Fe_3O_4 nanopowder through one-step thermal decomposition of $[Fe(NH_2CONH_2)_6](NO_3)_3$ in TEG. The TEG molecules

play a key role in the formation of water-soluble, monodisperse Fe_3O_4 nanopowder. The main advantages of this method are as follows: (i) the preparation procedure is very simple, and (ii) the iron precursor ($[Fe(NH_2CONH_2)_6](NO_3)_3$) is a nontoxic chemical that can be easily synthesized from readily available $Fe(NO_3)_3 \cdot 9H_2O$ and NH_2CONH_2. These advantages imply that the method does not need an expensive and complicated unit to produce high performance Fe_3O_4 nanopowder.

Acknowledgments

This work was financially supported by National Natural Science Foundation of China (Grant no. 20861006) and the Natural Science Foundation of Inner Mongolia (Grant no. 2009MS0806).

References

[1] R. Hao, R. Xing, Z. Xu, Y. Hou, S. Gao, S. Sun, Synthesis, functionalization, and biomedical applications of multifunctional magnetic nanoparticles, Advanced Materials 22 (2010) 2729–2742.
[2] S. Guo, D. Li, L. Zhang, J. Li, E. Wang, Monodisperse mesoporous superparamagnetic single-crystal magnetite nanoparticles for drug delivery, Biomaterials 30 (2009) 1881–1889.
[3] A.K. Guptaa, M. Gupta, Synthesis and surface engineering of iron oxide nanoparticles for biomedical applications, Biomaterials 26 (2005) 3995–4021.
[4] P. Majewski, B. Thierry, Functionalized magnetite nanoparticles—synthesis, properties, and bio-applications, Critical Reviews in Solid State and Materials Sciences 32 (2007) 203–215.
[5] H.T. Hai, H. Kura, M. Takahashi, T. Ogawa, Facile synthesis of Fe_3O_4 nanoparticles by reduction phase transformation from γ-Fe_2O_3 nanoparticles in organic solvent, Journal of Colloid and Interface Science 341 (2010) 194–199.
[6] S. Wu, W. Jiang, X. Zhang, H. Sun, W. Zhang, J. Dai, L. Liu, X. Chen, F. Li, A sonochemical route for the encapsulation of drug in magnetic microspheres, Journal of Magnetism and Magnetic Materials 324 (2012) 124–127.
[7] W. Jiang, H.C. Yang, S.Y. Yang, H.E. Horng, J.C. Hung, Y.C. Chen, C.Y. Hong, Preparation and properties of superparamagnetic nanoparticles with narrow size distribution and biocompatible, Journal of Magnetism and Magnetic Materials 283 (2004) 210–214.
[8] Z.H. Zhou, J. Wang, X. Liu, H.S.O. Chan, Synthesis of Fe_3O_4 nanoparticles from emulsions, Journal of Materials Chemistry 11 (2001) 1704–1709.
[9] S. Ni, X. Wang, G. Zhou, F. Yang, J. Wang, Q. Wang, D. He, Size controlled and morphology tuned fabrication of Fe_3O_4 nanocrystals and their magnetic properties, Journal of Alloys and Compounds 505 (2010) 727–732.
[10] R. Abu Mukh-Qasem, A. Gedanken, Sonochemical synthesis of stable hydrosol of Fe_3O_4 nanoparticles, Journal of Colloid and Interface Science 284 (2005) 489–494.
[11] D. Gonzalez, A.G. Nasibulin, H. Jiang, P. Queipo, E.I. Kauppinen, Electrospraying of ferritin solutions for the production of monodisperse iron oxide nanoparticles, Chemical Engineering Communications 194 (2007) 901–912.
[12] S. Sun, H. Zeng, D.B. Robinson, S. Raoux, P.M. Rice, S.X. Wang, G. Li, Monodisperse MFe_2O_4 (M=Fe, Co, Mn) nanoparticles, Journal of the American Chemical Society 126 (2004) 273–279.
[13] J. Rockenberger, E.C. Scher, A.P. Alivisatos, A new nonhydrolytic single-precursor approach to surfactant-capped nanocrystals of transition metal oxides, Journal of the American Chemical Society 121 (1999) 11595–11596.
[14] T. Hyeon, S.S. Lee, J. Park, Y. Chung, H.B. Na, Synthesis of highly crystalline and monodisperse maghemite nanocrystallites without a size-selection process, Journal of the American Chemical Society 123 (2001) 12798–12801.
[15] S. Sun, H. Zeng, Size-controlled synthesis of magnetite nanoparticles, Journal of the American Chemical Society 124 (2002) 8204–8205.
[16] N.R. Jana, Y. Chen, X. Peng, Size- and shape-controlled magnetic (Cr, Mn, Fe, Co, Ni) oxide nanocrystals via a simple and general approach, Chemistry of Materials 16 (2004) 3931–3935.
[17] C. Feldmann, H.-O. Jungk, Polyol-mediated preparation of nanoscale oxide particles, Angewandte Chemie International Edition 40 (2001) 359–362.
[18] J. Wan, W. Cai, X. Meng, E. Liu, Monodisperse water-soluble magnetite nanoparticles prepared by polyol process for high-performance magnetic resonance imaging, Chemical Communications (2007) 5004–5006.
[19] W. Cai, J. Wan, Facile synthesis of superparamagnetic magnetite nanoparticles in liquid polyols, Journal of Colloid and Interface Science 305 (2007) 366–370.
[20] F. Hu, K.W. MacRenaris, E.A. Waters, T. Liang, E.A. Schultz-Sikma, A.L. Eckermann, T.J. Meade, Ultrasmall, water-soluble magnetite nanoparticles with high relaxivity for magnetic resonance imaging, Journal of Physical Chemistry C 113 (2009) 20855–20860.
[21] M.S. Lupin, G.E. Peters, Thermal decomposition of aluminum, iron and manganese complexes of urea, Thermochimica Acta 73 (1984) 79–87.
[22] P. Wu, J. Zhu, Z. Xu, Template-assisted synthesis of mesoporous magnetic nanocomposite particles, Advanced Functional Materials 14 (2004) 345–351.
[23] S. Asuha, S. Zhao, H.Y. Wu, L. Song, O. Tegus, One step synthesis of maghemite nanoparticles by direct thermal decomposition of Fe–urea complex and their properties, Journal of Alloys and Compounds 472 (2009) L23–L24.
[24] C.R.D. Silva, S. Smith, I. Shim, J. Pyun, T. Gutu, J. Jiao, Z. Zheng, Lanthanide (III)-doped magnetite nanoparticles, Journal of the American Chemical Society 131 (2009) 6336–6337.
[25] J. Lu, X. Jiao, D. Chen, W. Li, Solvothermal synthesis and characterization of Fe_3O_4 and γ-Fe_2O_3 nanoplates, Journal of Physical Chemistry C 113 (2009) 4012–4017.
[26] T. Yamashita, P. Hayes, Analysis of XPS spectra of Fe^{2+} and Fe^{3+} ions in oxide materials, Applied Surface Science 254 (2008) 2441–2449.
[27] S. Zhao, H.Y. Wu, L. Song, O. Tegus, S. Asuha, Preparation of γ-Fe_2O_3 nanopowders by direct thermal decomposition of Fe–urea complex: reaction mechanism and magnetic properties, Journal of Materials Science 44 (2009) 926–930.
[28] K.S.W. Sing, D.H. Everett, R.A.W. Haul, L. Moscou, R.A. Pierotti, J. Rouquérol, T. Siemieniewska, Reporting physisorption data for gas/solid systems with special reference to the determination of surface area and porosity, Pure and Applied Chemistry 57 (1985) 603–619.
[29] Z. Huang, F. Tang, Preparation, structure, and magnetic properties of mesoporous magnetite hollow spheres, Journal of Colloid and Interface Science 281 (2005) 432–436.
[30] A. Angermann, J. Töpfer, Synthesis of magnetite nanoparticles by thermal decomposition of ferrous oxalate dehydrate, Journal of Materials Science 43 (2008) 5123–5130.
[31] X. Wei, Z. Wei, L. Zhang, Y. Liu, D. He, Highly water-soluble nanocrystal powders of magnetite and maghemite coated with gluconic acid: preparation, structure characterization, and surface coordination, Journal of Colloid and Interface Science 354 (2011) 76–81.
[32] H. Xia, J. Yi, P. Foo, B. Liu, Facile fabrication of water-soluble magnetic nanoparticles and their spherical aggregates, Chemistry of Materials 19 (2007) 4087–4091.
[33] M.P. Morales, S. Veitemillas-Verdaguer, M.I. Montero, C.J. Serna, A. Roig, L.L. Casas, B. Martínez, F. Sandiumenge, Surface and internal spin canting in γ-Fe_2O_3 nanoparticles, Chemistry of Materials 11 (1999) 3058–3064.